Scientific Research Publishing

American Journal of Analytical Chemistry, 2022, 13, 415-430
https://www.scirp.org/journal/ajac
ISSN Online: 2156-8278
ISSN Print: 2156-8251

Nucleation and Growth of Thallium on Thin Film Mercury Electrode: Voltammetric, Scanning Electron Microscopy, Chronoamperometric and Electrochemical Impedance Studies

Abdoulkadri Ayouba Mahamane[1,2*], Boubié Guel[2], Paul-Louis Fabre[3]

[1]Laboratoire Matériaux, Eaux, Environnement (LAMEE), Faculté des Sciences et Techniques, Université Abdou Moumouni, Niamey, Niger
[2]Laboratoire de Chimie Moléculaire et des Matériaux, Equipe Chimie Physique et Electrochimie, Département de Chimie, Université Joseph KI ZERBO, Ouagadougou, Burkina Faso
[3]Unité Mixte de Recherche (UMR CNRS 5503), Laboratoire de Génie Chimique, Toulouse, France
Email: *kadayouba@gmail.com

How to cite this paper: Mahamane, A.A., Guel, B. and Fabre, P.-L. (2022) Nucleation and Growth of Thallium on Thin Film Mercury Electrode: Voltammetric, Scanning Electron Microscopy, Chronoamperometric and Electrochemical Impedance Studies. *American Journal of Analytical Chemistry*, **13**, 415-430.
https://doi.org/10.4236/ajac.2022.1311028

Received: October 5, 2022
Accepted: November 6, 2022
Published: November 9, 2022

Abstract

Thallium is a heavy metal highly toxic to the biosphere. It can be determined by anodic stripping voltammetry after deposition on mercury film. The aim of this work is to study the conditions and mechanisms of deposition of Hg on glassy carbon electrode and Tl on Hg film by cyclic voltammetry, scanning electron microscopy, chronoamperometry and impedance techniques. The results showed a germination and growth of a 3D Hg phase on glassy carbon electrode. Similarly, the electrodeposition of Tl on Hg follows a 3D three-dimensional nucleation with diffusion controlled growth. The impedance measurements reveal an easier charge transfer on the Tl film.

Keywords

Thallium, Mercury Film, Cyclic Voltammetry, Scanning Electron Microscopy, Impedance Measurements

1. Introduction

The electrodeposition of metal (Me) films on a foreign substrate (S) has been extensively studied from a fundamental and applied view point, with applications in areas such as electroplating, thin film synthesis, microelectronics and

electroanalysis [1]. Electrochemical deposition and dissolution of metals can be generally expressed by:

$$\mathrm{Me}_{\mathrm{solv}}^{z+}(\mathrm{El}) \rightleftharpoons \mathrm{Me}^{z+}(\mathrm{Me}) \tag{1}$$

where $Me^{z+}(El)$ represents the metal ions in the electrolyte phase (El) and $Me^{z+}(Me)$ denotes the metal ions in the metal bulk phase (Me), which are coupled to the electrons $e^{-}(Me)$ in the Me-crystal lattice ($Me^{z+}(Me) + ze^{-}(Me) \rightleftharpoons Me$). At the so-called Nernst potential $E_{Me^{z+}/Me}$, $Me_{solv}^{z+}(El)$ and $Me^{z+}(Me)$ are in equilibrium, which is defined by the equality of the corresponding electrochemical potentials [1]. Mechanism of metal electrodeposition on foreign substrates (S) depends strongly on the Me-S interaction [2]. In systems with weak Me-S interaction (weak adhesion) metal deposition starts at supersaturation in the so-called overpotential deposition (OPD) range $E < E_{Me^{z+}/Me}$ with nucleation and growth of the 3D Me bulk phase. In the case of a strong Me-S interaction (strong adhesion), however, the deposition process can start even at undersaturation in the so-called underpotential deposition (UPD) range $E > E_{Me^{z+}/Me}$ with formation of low-dimensional metal phases (1D, 2D), which act as precursors for the nucleation and growth of the 3D Me bulk phase in the OPD range [1]. Nucleation and nuclei growth are the most important stage in the electrodeposition of a metal on a substrate S. Indeed, these two processes compete and influence the particle size of the deposited metal. The overall appearance and structure of the deposit are determined by the shape of the growth of the 3D nuclei electroplated on the substrate (S). Knowledge of the mechanism and kinetics of the formation of the first metal seeds electrodeposited on the conductive substrate S helps to understand the texture of the deposit on this substrate, whether it is a thin or thick deposit [3] [4].

Thallium (Tl) is considered to be a part of toxic heavy metals group with a high density value of 11.83 $g{\cdot}cm^{-3}$. Environmental exposure of Tl(I) includes both natural and anthropogenic activities. Thallium salts are widely spread in earth's layer with concentration ranging from 0.1 to 1 $mg{\cdot}kg^{-1}$ [5]. The determination of thallium is of primordial interest because despite its clinical, environmental and industrial applications [6], it is highly toxic for the biosphere. Its toxicity is even greater than that of mercury, cadmium, lead and copper [7].

Various analytical techniques are being employed for the determination of thallium such as Inductively Coupled Plasma (ICP), X-ray fluorescence (XRF) and Flame Atomic Absorption (FAA) Spectroscopy. But these techniques suffer from certain drawbacks like requirement of separate pre-concentration step, costly and bulky instrumentation. These techniques also lack speciation and simultaneous detection [8]. In recent years, electrochemical or voltammetric methods using anodic stripping voltammetry (ASV) or cathodic stripping voltammetry (CSV) have shown a high ability to detect trace heavy metals like thallium in environmental and biological matrices [9] [10]. Mercury drop electrodes were the first applications in this field. These involve application to a mercury drop electrode of a potential that increases linearly with time, relative to a reference

electrode [11]. However, the application of the mercury drop poses a problem for the environment due to its high and serious toxicity. For this reason, research has moved to the development of the mercury thin film and its application in methods (ASV and CSV). This development has the advantage of reducing the amount of mercury used in analytical procedures. Thus, mercuric ions Hg^{2+} are used, which, once pre-concentrated on the surface of a solid electrode, give the thin film of mercury. This film allows the metal cations to amalgamate. The solid electrode is generally glassy carbon (GCE) or carbon paste [12]. The processes involved are those of metallic electrodeposition on a foreign substrate. This study is of fundamental interest considering the clinical, environmental, and industrial applications of thallium [6]. Indeed, the optimal potential at which metal deposition takes place is related to the morphology and texture of the electrodeposited film. It is therefore important to understand the phenomena of thallium deposition on the solid substrate/mercury film, and to characterize the surfaces modified in this way by microscopic studies.

Despite its technological importance, electrodeposition of thallium on metal substrates has been the object of relatively few studies to date [13] [14] [15] [16] [17]. Basically, the lack of publications dealing with electrodeposition of Tl, through the last two decades is attributable to a higher toxicity of Tl and its compounds [13]. Labayen *et al. [14]* have worked on the initial stages of thallium electrodeposition on iodine-covered Pt(111) by cyclic voltammetry, low energy electron diffraction and Auger electron spectroscopy. Results show that the first electrodeposition peak corresponds to the deposition of 0.22 ML Tl atoms, independently of the structure of the initial iodine adlayer and thallium is retained on the surface in a stable structure. The characteristics of the electrodeposition of thallium powder from sulphate baths containing a relatively low Tl^{+} ion content (0.005 - 0.020 $mol{\cdot}L^{-1}$) were examined by Halim and co-worker [15]. According to the electrodeposition conditions, thallium powders were deposited in dendritic forms with different morphologies and grain sizes. Electrodeposition and characterization of thallium(III) oxide films were done by Liu *et al. [16]*. Tl_2O_3 films were electrodeposited onto ITO (indium tin oxide) substrates at different current densities. X-ray diffraction (XRD) studies reveal that the obtained film is amorphous at low electrodeposition current densities, while at high current densities it is polycrystalline. Scanning Electron Microscopy (SEM) observations show that the polycrystalline film grows at a preferred orientation vertical to the substrate, while the amorphous one exhibits no ordered growth. Scharifker [17] studied the catalytic reduction of nitrate during electrodeposition of thallium from Tl^{3+} solution. The voltammetric response of vitreous carbon electrodes in nitrate solution in the presence of Tl^{3+} shows the reduction of Tl^{3+} in two stages, to Tl^{+} and to metallic thallium, respectively Nitrate ions are reduced at high rates during the second stage, concurrently with Tl deposition.

All these studies reported gave information on the mechanisms and morphologies of thallium or oxide thallium deposited in particular conditions on various substrates. To the best of our knowledge, there are no studies on the

morphologies and impedance characteristics of deposition of thallium on mercury conducted.

In this paper we present new results on the conditions and mechanisms of electrodeposition of Hg on glassy carbon electrode and Tl on the mercury film by cyclic voltammetry, chronoamperometry, scanning electron microscopy (SEM) and characterization by electrochemical impedance spectroscopy.

2. Experimental

2.1. Electrodes, Instrumentation

The experimental set-up for cyclic voltammogram plots and chronoamperometry curves analysis is a Voltalab analytical Radiometer kit. It consists of a potentiostat PST050 and a polarographic stand MDE 150 comprising a measuring cell in which are placed:

1) A working electrode with an EDI 101 rotating disc having a glassy carbon tip (diameter 3 mm);

2) A silver chloride Ag/AgCl reference electrode, KClsat (potential 208 mV at 25˚C compared to the normal hydrogen electrode ENH);

3) A platinum auxiliary electrode;

4) An argon supply for solution bubbling.

The potentiostat and stand are controlled by a computer. The software used is Volta Master 4 for the execution of the commands as well as the data acquisition.

2.2. Reagents

All solutions were prepared with milli-Q water. Standard solutions were prepared from mercury nitrate (purity > 99.99%, Merck), thallium sulphate (purity > 99.995%, Sigma Aldrich) dissolved in 0.1 $mol{\cdot}L^{-1}$ perchloric acid $HClO_4$ (trace analysis) which was also used as the supporting electrolyte. A certified standard of thallium 1 $g{\cdot}L^{-1}$ (Certipur, Merck) was also used for the preparation of standard solutions. The solution was bubbled through a stream of pure argon.

2.3. Scanning Electron Microscopy (SEM) Analysis

The surface morphology of the electrodes was observed with a HITACHI TM-1000 Tabletop Microscope. It is coupled to an Energy Dispersive X-Ray Analysis (EDX) system. The measuring device is connected to a microcomputer which allows it to be controlled via the TM-1000 software for images and Swift ED-TM for elemental chemical analysis.

2.4. Chronoamperometry

The nucleation and growth kinetics of a 2D or 3D phase, during the deposition of a metal on a metallic or non-metallic substrate, is usually studied using $i = f(t)$ transients obtained by recording the evolution of the current density as a function of time during a potentiostatic control. The transients of the deposition of

Tl on Hg film were recorded at different final potentials E_f. The initial potential is maintained in all cases at $E_i = -400$ mV because at this potential there is no Tl deposition.

2.5. Impedance Measurements

Electrochemical impedance measurements were performed with the μAUTOLABIII/FRA system (Eco Chemie, Netherlands) driven by a microcomputer using the FRA (Frequency Response Analyser) software. All experiments were performed at room temperature. Measurements were made around the open circuit potential of the system by superimposing a minimum sinusoidal perturbation of 10 mV amplitude. The frequency range explored was from 50 mHz to 50 kHz.

3. Results and Discussion

3.1. Cyclic Voltammetry and SEM Analysis

Among the parameters affecting electrodeposition, the nature of the metal substrate, the electrolyte and the deposition potential play an important role [1]. Thus, cyclic voltammetry in the pure diffusion regime is used to identify the regions of deposition and dissolution potentials of a metal on a foreign substrate S [18]. The first system studied was the GCE/(Hg^{2+}, 10^{-3} mol·L^{-1}, supporting electrolyte $HClO_4$ 0.1 mol·L^{-1}) interface. The deposition of the mercury film on the GCE substrate is done with a mercuric ion solution of concentration Hg^{2+} 10^{-3} mol·L^{-1}. **Figure 1** shows the cyclic voltammogram corresponding to the deposition and redissolution of mercury on the GCE in 0.1 mol·L^{-1} $HClO_4$ medium at a scan rate of 40 mV/s. The potential scan is performed between 0.7 V and 0.2 V. The curve analysis shows that in the system under investigation, the formation of a monolayer (2D Hg phase) in the Under Potential Deposition (UPD) domain ($\Delta E = E - E_{Me^{z+}/Me} > 0$) can be excluded, indicating a relatively weak Hg deposit-substrate interaction. The hysteresis of the cathodic current in the Over Potential Deposition (OPD) domain, characterised by $\eta = E - E_{Me^{z+}/Me} < 0$, as well as the cross-over of the cathodic and anodic plots at the equilibrium potential of the Hg^{2+}/Hg system, $E^{\circ}_{Hg^{2+}/Hg} = 0.44$ V/ref, is related to the germination and growth of a 3D Hg phase that dissolves in the course of the anodic sweep back into the UPD domain [1] [19].

The SEM study allowed the observation of the Hg film on the surface of the glassy carbon electrode. The GCE substrate is first raised to a potential in the UPD range and then raised to a cathodic potential in the OPD range. **Figure 2** is a series of images showing the morphology of the electrodeposited film on the surface of the GCE substrate according to the routine polarisation described above. **Figure 2(a)** shows an SEM image of the GCE substrate prior to the deposition of a mercury film. A perfectly uniform surface is observed. The EDX analysis performed does not show any metallic elements. **Figure 2(b)** and **Figure 2(c)** show the surfaces of the GCE substrate after Hg deposition from a 10^{-3} mol·L^{-1} Hg^{2+} solution in 0.1 mol·L^{-1} $HClO_4$ medium at a potential of 0.2 V at a

given deposition time. The SEM image was taken after a deposition time of 2 min (**Figure 2(b)**) shows sparse granules on the electrode surface. The Hg deposition is in the form of random crystallites on the substrate surface, confirming the weak metal-substrate interaction. These observed 3D growth islets and the absence of 2D Hg phases indicate that the electrodeposition of Hg on the GCE can be described by the so-called "Volmer-Weber" growth mechanism or islet growth mode. At a deposition time of 4 min, the SEM image (**Figure 2(c)**) shows a compact film of mercury. This is in fact a surface uniformly covered by grains arranged against each other and which constitute the texture of the mercury film. This texture of mercury films has already been reported in the literature [20] [21] [22]. Energy Dispersive X-ray (EDX) analysis of a portion of this surface shows that it is well covered with Hg, the EDX analysis also revealing the presence of chlorine from the 0.1 mol·L^{-1} $HClO_4$ supporting electrolyte. The experimental conditions retained for the deposition of Hg on the GCE substrate are therefore the following: deposition potential 0.2 V/ref (Ag/AgCl, KClsat), deposition time equal to 4 min.

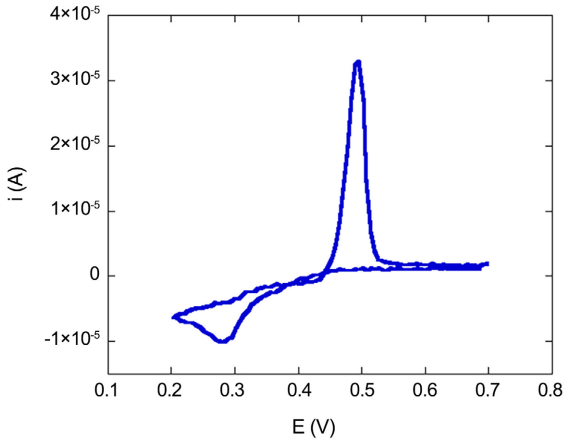

Figure 1. Cyclic voltammogram corresponding to the deposition and redissolution of Hg on GCE ([Hg^{2+}] = 10^{-3} mol·L^{-1}, supporting electrolyte $HClO_4$ 0.1 mol·L^{-1}, scan rate 40 mV/s; reference electrode Ag/AgCl, KClsat).

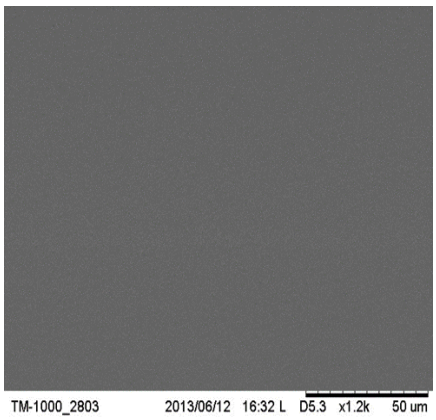

(a)

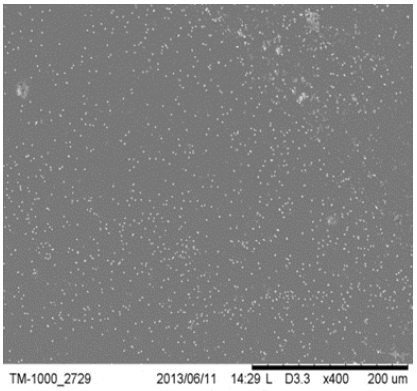

(b)

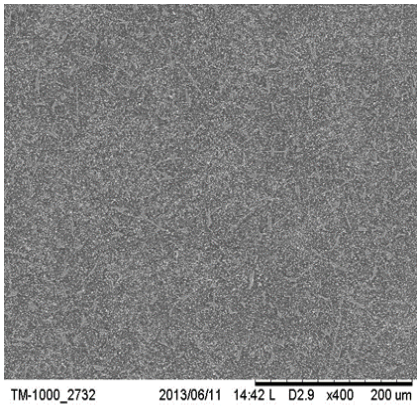

(c)

Figure 2. SEM images: (a) GCE before mercury deposition; (b) GCE after Hg deposition from a 10^{-3} mol·L^{-1} Hg^{2+} solution at 0.2 V for 2 min; (c) GCE after Hg deposition from a 10^{-3} mol·L^{-1} Hg^{2+} solution at 0.2 V for 4 min.

The second system studied was the interface GCE/Hg film/(Tl^+, concentration C, supporting electrolyte $HClO_4$ 0.1 mol·L^{-1}), C is the concentration of Tl^+ ions to be determined in an aqueous matrix. The investigations were first carried out for a Tl^+ ion concentration C equal to 10^{-3} mol·L^{-1}. **Figure 3** is a cyclic voltammogram corresponding to the deposition and redissolution of Tl on the mercury film at a scan rate of 2 mV/s. The hysteresis of the cathodic current is obtained at a cathodic potential below −0.9 V/ref and a cross-over of the cathodic and anodic plots at this potential. In contrast to the deposition of Hg on the GCE (**Figure 2**), the cross-over of the cathodic and anodic plots does not occur at the equilibrium potential of the Tl^+/Tl system. The equilibrium potential of the Tl^+/Tl system, $E^{\circ}_{Tl^+/Tl(Hg)} = -0.75$ V/ref, was measured in the open circuit cell. This value is identical to the potential at the intersection of the curve with the zero current axis. In a first approximation, the hysteresis of the cathodic current and the cross-over at the potential of −0.9 V/ref could indicate an increase in the density of 3D Tl nuclei and the growth of these nuclei in a potential range below −0.9 V/ref.

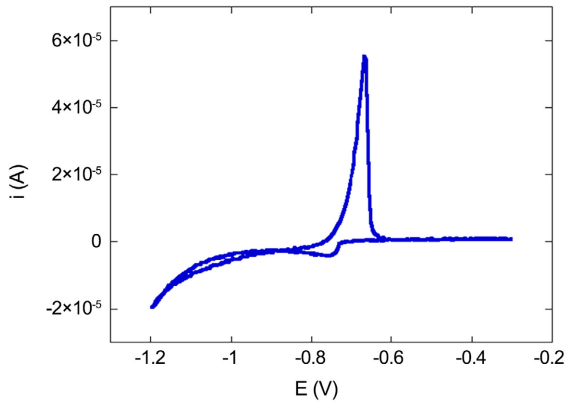

Figure 3. Cyclic voltammogram corresponding to the deposition and redissolution of Tl on Hg and showing a cross-over ($[Tl^+] = 10^{-3}$ mol·L^{-1}, $HClO_4$ supporting electrolyte 0.1 mol·L^{-1}, scan rate 2 mV/s, Ag/AgCl KClsat reference electrode).

In agreement with Nernst's law, the potential at which the cathodic and anodic plots cross is shifted towards the negative potentials when the concentration of Tl^+ ions increases from 10^{-6} to 10^{-3} mol·L^{-1}. Analysis of the curve does not reveal the formation of a 2D Tl phase. Before the cross-over potential, the electrochemical reaction corresponding to the incorporation of Tl^+ ions into the mercury amalgam is:

$$Tl^+ + e^- (Hg) \rightleftharpoons Tl(Hg) \quad (2)$$

This reaction is controlled by the diffusion of Tl^+ ions into the mercury amalgam. As mercury has no growth sites (imperfections, surface irregularities, etc.), the nucleation and growth processes of 3D Tl phases are inhibited in a first step. Subsequently, as the Tl film becomes compact, the surface is characterized by a higher density of imperfections or growth sites. The increase of the density of growth sites is significant after the cross-over potential. The nucleation of 3D Tl nuclei, followed by the growth of these nuclei, is then easier on the surface [23].

The influence of the scan rate (v) during Tl deposition was studied in the potential range −0.2 to −1 V, with the scan rate varying between 2 and 100 mV/s. The results are shown in **Figure 4**. It is important to note that at high scan speeds, the cross-over is no longer visible on the voltammograms.

The normalized voltammograms obtained by plotting $i.v^{-1/2} = f(E)$ show that in reduction all curves are superimposed. The reduction peak varies with the square root of the scan rate ($v^{1/2}$), which confirms the diffusion of Tl^+ ions in the mercury amalgam [24]. On the other hand, the oxidation does not vary with $v^{1/2}$, nor with v. The oxidation therefore goes through a limiting kinetic stage.

A series of Tl deposits on the GCE/Hg substrate were carried out at different potentials and the corresponding SEM images are shown in **Figure 5**. The GCE/Hg substrate is first raised to a potential in the range where Tl deposition does not take place, and then raised to a cathodic potential corresponding to the electrochemical reaction. At a potential of −0.7 V (**Figure 5(a)**), a few scattered particles are observed. EDX analysis, carried out on this surface, did not detect

Tl (84.9% Hg, 0% Tl and 15.1% Cl). At this potential, the Tl(Hg) amalgam consists mainly of mercury. The SEM image in **Figure 5(b)** corresponds to a Tl deposit at a potential of −1 V with a deposition time of 2 min. Considering that the increase in density of growth sites occurs below −0.9 V, it is expected to observe a larger population of Tl grains, stacked against each other, some of them being stick-shaped. At this potential, Tl deposition takes place on a surface consisting mainly of Hg grains. By extending the deposition time to 4 min at a potential of −1 V, we find that the surface is almost covered with a Tl film, indicating the formation of tree-like branches (**Figure 5(c)**). Indeed, the EDX analysis carried out on this surface reveals a massive Tl deposit (100%). At a potential of −1.2 V for 4 min, a surface more or less covered by sheets can be observed on the SEM image of **Figure 5(d)**, still indicating tree-like ramifications. However, this surface is much less covered than at the −1 V potential. This result is confirmed by the EDX analysis, which shows a lower deposition than at −1 V, *i.e.* 80.7% Tl. This result can be explained if we consider that below −1 V, the reduction of protons starts to be important and therefore decreases the quantity of Tl deposited on the surface [25].

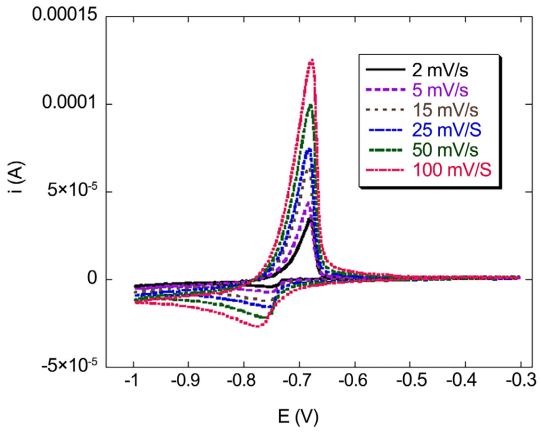

Figure 4. Cyclic voltammograms of the GCE/Hg/Tl^+ system as a function of scan speed ($[Tl^+] = 10^{-3}$ mol·L^{-1}, Supporting electrolyte $HClO_4$ 0.1 mol·L^{-1}, reference electrode Ag/AgCl KClsat).

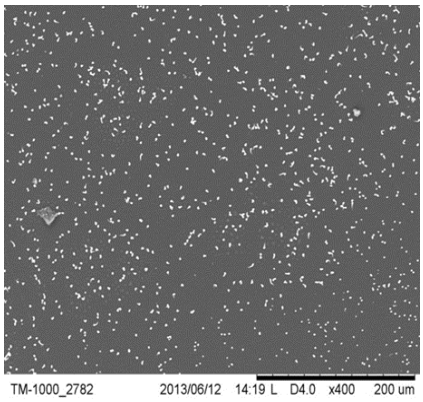

(a)

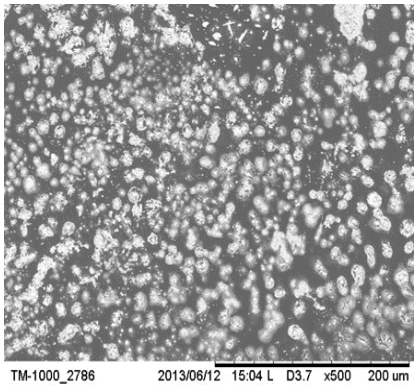

(b)

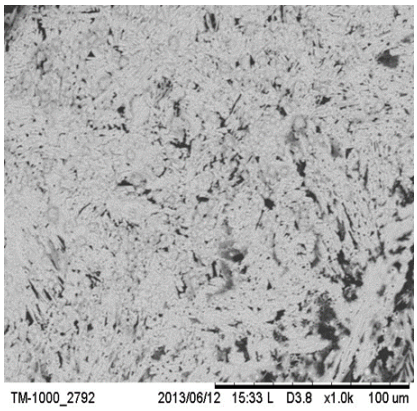

(c)

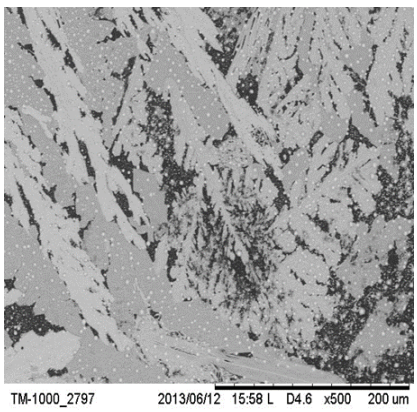

(d)

Figure 5. SEM images: (a) Tl deposition from a 10^{-3} mol·L^{-1} Tl^{+} solution at −0.7 V for 4 min; (b) Tl deposition from a 10^{-3} mol·L^{-1} Tl^{+} solution at −1 V for 2 min; (c) Tl deposition from a Tl^{+} 10^{-3} mol·L^{-1} solution at −1 V for 4 min; (d) Tl deposition from a Tl^{+} 10^{-3} mol·L^{-1} solution at −1.2 V for 4 min.

3.2. Chronoamperometry

The growth kinetics were studied by potentiostatic transient methods. These transients characterize the deposition of Tl on Hg. **Figure 6** shows these transients in a representation $-i = f(t)$.

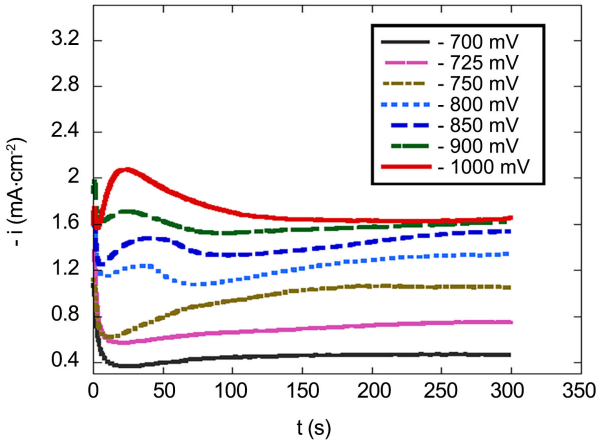

Figure 6. Current-time transients for the deposition process of Tl on ECV/Hg at different values of E_f (E_i = −400 mV) ([Tl^+] = 5 × 10^{-3} mol·L^{-1}, supporting electrolyte $HClO_4$ 0.1 mol·L^{-1}).

The transients at −700 mV and −725 mV are monotonic decreasing, indicating diffusion controlled kinetics. They correspond to the Tl(Hg) amalgam formation reaction and no 3D nuclei formation can be envisaged at these potentials. The transients pass through a maximum, starting at a potential of −800 mV. The time to reach this maximum decreases as the potential becomes more negative. Thus, at a potential of −1000 mV, there is a well-defined maximum characteristic of a nucleation and three-dimensional growth mechanism [23] [26] [27].

A theoretical model taking into account the overlap of diffusion zones has been proposed by Sharifker *et al.* [23]. **Figure 7** shows the theoretical model curves $(i/i_m)^2$ versus (t/t_m) for 3D progressive and instantaneous nucleation and an experimental curve $(i/i_m)^2$ versus (t/t_m). The experimental curve in **Figure 7** was obtained from the transient at the −1000 mV potential. The experimental curve fits perfectly with the theoretical model corresponding to progressive nucleation. It can therefore be concluded that at this potential of −1000 mV, the nucleation of 3D Tl nuclei is progressive. This result is in agreement with the microscopic study which showed that at this potential, we have a quasi-covered surface of a thallium film with a high density of growth sites.

3.3. Electrochemical Impedance Study

Impedance measurements were carried out to characterize the interface GCE/Hg film/Tl film/(Tl^+, concentration C, supporting electrolyte $HClO_4$ 0.1 mol·L^{-1}). This system represents the electrochemical sensor that will be used for the quantitative determination of Tl^+ ions in aqueous solution. The bare GCE and the GCE covered with a mercury film had to be characterized first. All the curves obtained are shown in **Figure 8**.

The impedance diagram of the bare GCE is recorded in the 0.1 mol·L^{-1} $HClO_4$ supporting electrolyte and in a solution of the supporting electrolyte containing

the mercuric ions Hg^{2+} 10^{-3} mol·L^{-1}. The impedance diagrams (in Nyquist representation) obtained are identical and overlap perfectly (**Figure 8(a)**). The charge transfer resistance, measured by evaluating the diameter of the semi-circle corresponding to the transfer loop, is 1.53 × 10^7 Ω (Ohm). This high resistance obtained for the bare GCE reflects that when no electroactive redox couple is present, there is no charge transfer reaction at the electrode. In contrast, when a mercury film is electrodeposited on the GCE at a potential of 0.2 V for 4 min and the impedance diagram is recorded in the 0.1 mol·L^{-1} $HClO_4$ supporting electrolyte solution containing 10^{-3} mol·L^{-1} Hg^{2+} ions (**Figure 8(b)**), we obtain a decreasing charge transfer resistance as expected: it goes from 1.53 × 107 Ω for the GCE/(Hg^{2+} 10^{-3} mol·L^{-1}, $HClO_4$ 0.1 mol·L^{-1}) system to 4.66 × 10^6 Ω for the GCE/Hg film/(Hg^{2+} 10^{-3} mol·L^{-1}, $HClO_4$ 0.1 mol·L^{-1}) system. This decrease is related to the charge transfer reaction at the electrode [22] [27] [28].

The deposition of thallium on the ECV/mercury film is carried out for 4 min at a potential of −1 V. The impedance diagram is then recorded for the ECV/Hg film/Tl film system (Tl^+ 10^{-3} mol·L^{-1}, $HClO_4$ 0.1 mol·L^{-1}) (**Figure 8(c)**). In pure diffusion regime, in the high frequency range, the capacitive loop is not clearly visible and this is due to the fact that the electron transfer is very fast. The Warburg line is mainly observed at medium and low frequencies. The Warburg impedance (W) has a value of 7.4 × 10^{-4} Ω·$s^{-1/2}$. The resistance of the solution is 55 Ω. The charge transfer resistance decreases significantly from 4.66 × 10^6 Ω for the GCE/Hg film/(Hg^{2+} 10^{-3} mol/L, $HClO_4$ 0.1 mol·L^{-1}) system to a value of 2290 Ω for the GCE/Hg film/Tl/(Tl^+ 10^{-3} mol·L^{-1}, $HClO_4$ 0.1 mol·L^{-1}) system. These results, compiled in **Table 1**, can be easily explained if one considers that the charge transfer is made easier on the Tl film [29] [30] [31]; this was also shown in the SEM analysis.

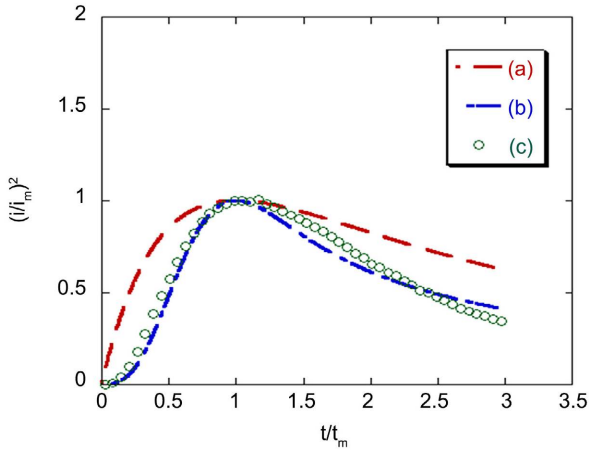

Figure 7. Adimensional transients: (a) Instantaneous nucleation; (b) Progressive nucleation; (c) Experimental points for E_f = −1000 mV. With: i_m the maximum current measured on the curve $i = f(t)$ and tm the time at which i_m is measured on the curve $i = f(t)$ ([Tl^+] = 5.10^{-3} mol·L^{-1}, support electrolyte $HClO_4$ 0.1 mol·L^{-1}).

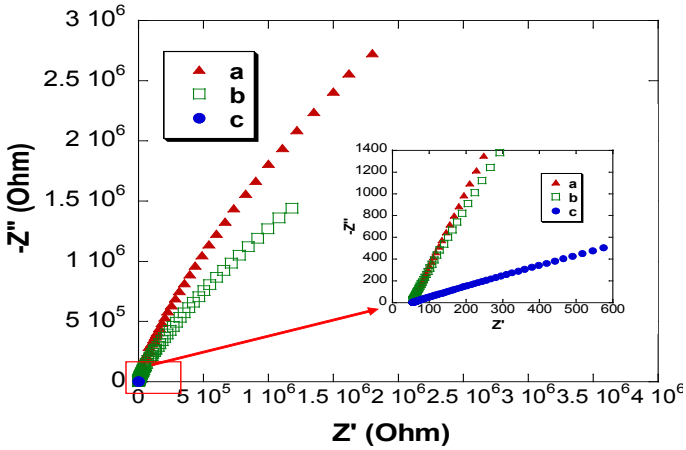

Figure 8. Nyquist steady state plots: (a) bare GCE; (b) Hg-coated GCE, ($[Hg^{2+}]$ = 10^{-3} mol·L^{-1}, supporting electrolyte $HClO_4$ 0.1 mol·L^{-1}, Hg deposition potential 0.2 V, Hg deposition time 4 min, electrode rotation 1000 revolutions per minute (rpm)); (c) deposition of Tl on ($[Tl^{+}]$ = 10^{-3} mol·L^{-1}, supporting electrolyte $HClO_4$ 0.1 mol·L^{-1}, deposition potential of Tl −1000 mV, deposition time of Tl 4 min, electrode rotation 1000 rpm).

Table 1. Electrochemical impedance spectroscopy results.

System	Charge transfert resistance Rct (Ω)
GCE/Hg^{2+}	1.53×10^7
$GCE/Hg/Hg^{2+}$	4.66×10^6
$GCE/Hg/Tl/Tl^{+}$	2290

4. Conclusion

The techniques of cyclic voltammetry, Electrochemical Impedance Spectroscopy (EIS) and SEM analysis coupled with EDX analysis gave information on the deposition and dissolution potentials, the surface state of the electrodes and the chemical composition. The mercury deposit shows small grains arranged against each other giving the appearance of a film. The EIS results confirm the SEM observations. For the Tl deposit on Hg, a rather rough surface is observed in SEM. This system (GCE/HG film/Tl^{+}, C) studied will further be used for the quantitative determination of Tl^{+} ions in aqueous matrices.

Acknowledgements

This work was sponsored by the International Science Program (ISP/IPICS) Uppsala, Sweden. Their financial support is gratefully acknowledged. Abdoulkadri Ayouba Mahamane would like to thank the ISP/IPICS for receiving fellowships to stay at the University of Toulouse (Laboratoire de Génie Chimique). This work was also made possible within the framework of the Institutional cooperation "FRI-OR" between the University of Paul Sabatier-Toulouse III (France) and the University Joseph Ki-Zerbo of Ouagadougou (Burkina Faso).

Conflicts of Interest

The authors declare no conflicts of interest regarding the publication of this paper.

References

[1] Krumm, R., Guel, B., Schmitz, C. and Staikov, G. (2000) Nucleation and Growth in Electrodeposition of Metals on n-Si(111). *Electrochimica Acta*, **45**, 3255-3262. https://doi.org/10.1016/S0013-4686(00)00418-7

[2] Geng, L., Liu, Q., Chen, J., Jia, P., Ye, H., Yan, J., *et al.* (2021) *In Situ* Observation of Electrochemical Ostwald Ripening during Sodium Deposition. *Nano Research*, **15**, 2650-2654. https://doi.org/10.1007/s12274-021-3861-6

[3] Dang, T.K., Van Toan, N., Hung, C.M., Van Duy, N., Viet, N.N., Thong, L.V., *et al.* (2022) Investigation of Zinc Electronucleation and Growth Mechanisms onto Platinum Electrode from a Deep Eutectic Solvent for Gas Sensing Applications. *Journal of Applied Electrochemistry*, **52**, 299-309. https://doi.org/10.1007/s10800-021-01635-0

[4] Bahar, J., Lghazi, Y., Youbi, B., Himi, M.A., El Haimer, C., Ouedrhiri, A., *et al.* (2022) Nucleation and Growth Mechanism of Cuprous Oxide Electrodeposited on ITO Substrate. *Materials Today*: *Proceedings*, **66**, 187-195. https://doi.org/10.1016/j.matpr.2022.04.445

[5] Zhong, Q., Qi, J., Liu, J., Wang, J., Lin, K., Ouyang, Q., *et al.* (2022) Thallium Isotopic Compositions as Tracers in Environmental Studies: A Review. *Environment International*, **162**, Article ID: 107148. https://doi.org/10.1016/j.envint.2022.107148

[6] Çolak, H. and Mercan, H.İ. (2022) Influence of Thallium Doping on Structural, Electrical, and Optical Properties of ZnO Nanorods for TCO Applications. *Journal of Materials Science*: *Materials in Electronics*, **33**, 14816-14828. https://doi.org/10.1007/s10854-022-08401-8

[7] Blain, R. (2022) Thallium. In: Nordberg, G.F. and Costa, M., Eds., *Handbook on the Toxicology of Metals*, Academic Press, Cambridge, 795-806. https://doi.org/10.1016/B978-0-12-822946-0.00028-3

[8] Lochab, A., Saxena, M., Jindal, K., Tomar, M., Gupta, V. and Saxena, R. (2021) Thiol-Functionalized Multiwall Carbon Nanotubes for Electrochemical Sensing of Thallium. *Materials Chemistry and Physics*, **259**, Article ID: 124068. https://doi.org/10.1016/j.matchemphys.2020.124068

[9] Ma, S., Zhao, G., Elsayed, M., Sedki, M., Chen, X., Wu, D., *et al.* (2021) Toward Rapid Detection of Trace Lead and Cadmium by Anodic Stripping Voltammetry in Complex Wastewater Streams. *ACS ES&T Engineering*, **1**, 1509-1516. https://doi.org/10.1021/acsestengg.1c00161

[10] Pardi, H., Deswati, D., Edelwis, T.W., Willian, N. and Fitriyah, D. (2021) Differential Pulse Adsorptive Cathodic Stripping Voltammetry for the Simultaneous Determination of Pb and Zn in Seawater Using Calcon. *Portugaliae Electrochimica Acta*, **39**, 45-57. https://doi.org/10.4152/pea.202101045

[11] Rahm, C.E., Gupta, P., Gupta, V.K., Huseinov, A., Griesmer, B. and Alvarez, N.T. (2022) Impact of Physical and Chemical Parameters on Square Wave Anodic Stripping Voltammetry for Trace Pb^{2+} Detection in Water. *Analyst*, **147**, 3542-3557. https://doi.org/10.1039/D2AN00724J

[12] El-Khouly, A.A., Hafez, M.A.H. and Kenawy, I.M.M. (2006) Kinetics and Thermodynamics of the Electrodeposition of Palladium, Thallium, and Tellurium from

Different Baths. *Russian Journal of Electrochemistry*, **42**, 225-232. https://doi.org/10.1134/S1023193506030037

[13] Malik, A.S., Boyko, O., Atkar, N. and Young, W.F. (2001) A Comparative Study of MR Imaging Profile of Titanium Pedicle Screws. *Acta Radiologica*, **42**, 291-293. https://doi.org/10.1080/028418501127346846

[14] Labayen, M. and Harrington, D.A. (2004) Initial Stages of Thallium Electrodeposition on Iodine-Covered Pt(111). *Journal of Electroanalytical Chemistry*, **567**, 185-192. https://doi.org/10.1016/j.jelechem.2003.12.023

[15] Abd El-Halim, A.M. and Khalil, R.M. (1984) Electrodeposition of Thallium Powder from Sulphate Baths. *Surface Technology*, **23**, 215-223. https://doi.org/10.1016/0376-4583(84)90014-1

[16] Liu, J.-F., Wang, S.-X., and Yang, K.-Z. (1997) Electrodeposition and Characterization of Thallium(III) Oxide Films. *Thin Solid Films*, **298**, 156-159. https://doi.org/10.1016/S0040-6090(96)09169-9

[17] Scharifker, B. (2000) Catalytic Reduction of Nitrate during Electrodeposition of Thallium from Tl^{3+} Solution. *Electrochemistry Communications*, **2**, 448-451. https://doi.org/10.1016/S1388-2481(00)00052-7

[18] Momčilović, M.Z. (2022) Recent Innovations in Voltammetric Techniques. In: Manjunatha, J.G., Ed., *Electrochemical Sensors Based on Carbon Composite Materials*, IOP Publishing, Bristol, 6-1-6-22. https://doi.org/10.1088/978-0-7503-5127-0ch6

[19] Shao, W., Sun, Y., Xu, Y. and Zangari, G. (2022) Depolarization of Cu Electrodeposition in the Presence of Ag: A Cyclic-Voltammetry Study. *Electrochimica Acta*, **405**, Article ID: 139796. https://doi.org/10.1016/j.electacta.2021.139796

[20] Jovanovski, V., Xhanari, K. and Finšgar, M. (2022) Editorial: Recent Advances of Metal-Film Electrodes for Trace Electrochemical Analysis. *Frontiers in Chemistry*, **10**, Article ID: 973672. https://doi.org/10.3389/fchem.2022.973672

[21] Grosser, T., Wehrhold, M., Neubert, T.J. and Balasubramanian, K. (2021). Graphene-Rcury-Aphene Sandwich Electrode for Electroanalysis. *ChemElectroChem*, **8**, 4277-4285. https://doi.org/10.1002/celc.202101290

[22] Sherigara, B.S., Shivaraj, Y., Mascarenhas, R.J. and Satpati, A.K. (2007) Simultaneous Determination of Lead, Copper and Cadmium onto Mercury Film Supported on Wax Impregnated Carbon Paste Electrode: Assessment of Quantification Procedures by Anodic Stripping Voltammetry. *Electrochimica Acta*, **52**, 3137-3142. https://doi.org/10.1016/j.electacta.2006.09.055

[23] Scharifker, B. and Hills, G. (1983) Theoretical and Experimental Studies of Multiple Nucleation. *Electrochimica Acta*, **28**, 879-889. https://doi.org/10.1016/0013-4686(83)85163-9

[24] Kim, G.W. and Ha, J.W. (2022) Single-Particle Study on Hg Amalgamation Mechanism and Slow Inward Diffusion in Mesoporous Silica-Coated Gold Nanorods without Structural Deformation. *The Journal of Physical Chemistry Letters*, **13**, 2607-2613. https://doi.org/10.1021/acs.jpclett.2c00189

[25] Ferrari, A.G.M., Crapnell, R.D., Adarakatti, P.S., Suma, B.P. and Banks, C.E. (2022) Electroanalytical Overview: The Detection of Chromium. *Sensors and Actuators Reports*, **4**, Article ID: 100116. https://doi.org/10.1016/j.snr.2022.100116

[26] Carboney, A.S., Crespo-Yapur, D.A. and Videa, M. (2022) Mathematical Analysis of Cyclic and Sampled Current Voltammetries for the Description of Nucleation and Growth Processes of Metallic Nanoparticles. *ECS Transactions*, **106**, Article No. 3. https://doi.org/10.1149/10601.0003ecst

[27] Bahrololoomi, A., Bilan, H.K. and Podlaha, E.J. (2022) Electrodeposited Ni-Fe onto Glassy Carbon for the Detection of Methylene Blue. *Journal of the Electrochemical Society*, **169**, Article ID: 012501. https://doi.org/10.1149/1945-7111/ac429e

[28] Brett, C.M. (2022) Electrochemical Impedance Spectroscopy in the Characterisation and Application of Modified Electrodes for Electrochemical Sensors and Biosensors. *Molecules*, **27**, Article No. 1497. https://doi.org/10.3390/molecules27051497

[29] Liu, Y., Xue, Q., Chang, C., Wang, R., Wang, Q. and Shan, X. (2022) Highly Efficient Detection of Cd (II) Ions by a Stannum and Cerium Bimetal-Modified Laser-Induced Graphene Electrode in Water. *Chemical Engineering Journal*, **433**, Article ID: 133791. https://doi.org/10.1016/j.cej.2021.133791

[30] Maciel, C.C., de S.M. Freitas, A., Medrades, J.P. and Ferreira, M. (2022) Simultaneous Determination of Catechol and Paraquat Using a Flexible Electrode of PBAT and Graphite Modified with Gold Nanoparticles and Copper Phthalocyanine (g-PBAT/AuNP/CuTsPc) LbL Film. *Journal of the Electrochemical Society*, **169**, Article ID: 027505. https://doi.org/10.1149/1945-7111/ac4ff0

[31] Antherjanam, S. and Saraswathyamma, B. (2022) Simultaneous Electrochemical Determination of Hydrazine and Hydroxylamine on a Thiadiazole Derivative Modified Pencil Graphite Electrode. *Materials Chemistry and Physics*, **275**, Article ID: 125223. https://doi.org/10.1016/j.matchemphys.2021.125223